Phase front shapes and thermal distributions for KD_2PO_4 samples in a rotating thermal gradient

1996 J. Phys.: Condens. Matter 8 7365

(http://iopscience.iop.org/0953-8984/8/39/013)

J. Phys.: Condens. Matter **8** (1996) 7365–7377. Printed in the UK

Phase front shapes and thermal distributions for KD_2PO_4 samples in a rotating thermal gradient

Jean Bornarel†, Ryszard Cach‡ and Zdenek Kvitek†

† Laboratoire de Spectrométrie Physique, (UMR 5588) Université Joseph Fourier, BP 87, 38402 Saint-Martin-d'Hères Cédex, France

‡ Institute of Experimental Physics, University of Wroclaw, pl. Maxa Borna 9, 50-205 Wroclaw, Poland

Received 11 January 1996, in final form 9 April 1996

Abstract. The shape of the DKDP phase front is observed along three perpendicular directions during the coexistence of the paraelectric and ferroelectric phases for different orientations of an external thermal gradient $\boldsymbol{G}_e$. Quasi-planar and zigzag shapes are then described. The thermal distribution inside the sample can be well represented by a thermal gradient $\boldsymbol{G}_i$ in the middle of a non-plate-shaped sample. The important effect of the sample's corners is also demonstrated.

1. Introduction

At a temperature of around 215 K, KD_2PO_4 (DKDP) crystals exhibit a first-order transition between a tetragonal paraelectric phase ($\bar{4}2d$) which is the high-temperature phase, and an orthorhombic ferroelectric and ferroelastic phase ($mm2$). The ferroelectric domains appearing in the low-temperature phase have not been studied as much as in KH_2PO_4 (KDP) (Bornarel 1987) but they look alike with permissible walls in (100) and (010) tetragonal planes (Fousek and Janovec 1969). These domains are also mechanical twins and the importance of the mechanical energy in the domain texture of KDP-type crystals has long since been known (Bornarel and Lajzerowicz 1968, Bornarel 1972). The DKDP transition was studied by means of macroscopic measurements such as specific heat (Strukov *et al* 1968), dielectric susceptibility (Strukov *et al* 1972), polarization measurements (Sidnenko and Gladkii 1973), dielectric and electrocalorific properties (Reese 1969) and also x-rays (Andrews and Cowley 1986) or neutrons (Nelmes *et al* 1985). Diffraction studies provide information covering the whole sample.

The first information on the phase front was produced through interpretation of neutron diffraction measurements (Zeyen *et al* 1976); these workers suggested that, during the phase coexistence, paraelectric and ferroelectric stripes perpendicular to the c ferroelectric axis alternate in the sample. The validity of this prediction was confirmed by synchrotron x-ray topographies (Aleshko-Orzhevskii 1982, 1983, 1992) and optical observations (Bachheimer *et al* 1981). These results demonstrated the greater importance, for the phase front orientation, of elastic energy in relation to electrostatic energy: electrostatic energy is minimized by a phase front parallel to c which avoids the charges on the front. Elastic energy would be minimized by a phase front orientation perpendicular to c if a simple model based on the work by Khatchaturyan (1967) and Bastie *et al* (1980) were used, essentially because the u_{xx}- and u_{yy}-values (10^4) are lower than the u_{zz}-value (6.5×10^{-4})

0953-8984/96/397365+13$19.50

(Zeyen *et al* 1976). Other models could obviously be applied to this mechanical energy minimization.

In the last few years, optical observations have been performed in transmitted light along the three axes of the tetragonal system simultaneously with dielectric measurements revealing different phase front shape possibilities such as daggers, zigzag or quasi-planar fronts (Bornarel and Cach 1991, 1993, 1994). Some results are interesting and need to be studied thoroughly as the fact that, at the beginning of the coexistence in a paraelectric–ferroelectric (PF) transition, the dielectric constant along the c axis still follows approximately the paraelectric Curie–Weiss law, and the ferroelectric region seems to be of a monodomain nature (Bornarel and Cach 1993, 1994). Phenomena in a phase coexistence are strongly dependent on experimental conditions such as thermal gradients $\boldsymbol{G}_e$. A recent paper explains in detail what happens when $\boldsymbol{G}_e$ and $\boldsymbol{c}$ are parallel (Bornarel and Cach 1994): the phase front has a quasi-planar shape and is nearly perpendicular to the c axis. The variation in the dielectric constant during the phase coexistence has been described with the help of a phenomenological model which demonstrates the contribution of the domains. Then a more general study of the influence of the thermal gradient on the DKDP phase transition has been performed with a thermal gradient $\boldsymbol{G}_e$ of constant magnitude and changing orientation, and also with $\boldsymbol{G}_e$ perpendicular to $\boldsymbol{c}$ axis and changing magnitude.

In the present paper, the phase coexistence is described for a DKDP sample under an external constant thermal gradient. The orientation of the sample varies, thus modifying the phase front shape. A simple model allows us to calculate the temperature distribution inside the sample and to discuss the physical observations. The dielectric measurements obtained in similar experimental conditions are reported and will be discussed in a subsequent paper.

2. Experimental procedures

The DKDP crystals were grown by slow cooling of a supersaturated solution of KDP and heavy water. The observed transition temperature corresponds to a deuteration concentration of 83%. The weak tapering angle of the crystal (a few degrees), the room-temperature optical studies and the dielectric properties lead us to conclude that the sample is of good quality. The sample was cut with a wire saw. The orientation of the sample was verified with x-rays (accuracy of a minute of arc) and each face was polished on a silk cloth with diamond paste. Semitransparent gold electrodes were evaporated on the c faces. The sample was placed in the helium gas exchange chamber of a cryostat, allowing optical observations in three perpendicular directions. The thermal gradient $\boldsymbol{G}_e$ existing in the vertical direction inside the helium gas exchange chamber is the consequence of the cryostat design with the upper part hotter than the bottom part. This orientation of the temperature gradient reduces the influence of the convection as experimentally verified. The magnitude of the temperature gradient is constant in the space corresponding to the dimension of sample and varies linearly with the temperature rate R as described in a previous paper (Bornarel and Cach 1994). The thermal gradient magnitude is constant for the results presented here and equal to 0.2 ± 0.01 K mm^{-1} with a temperature rate $|R|$ less than 10^{-2} K min^{-1}. The temperature may also be regulated with an accuracy of a few 10^{-3} K. Two thin copper wires (diameter equal to 5×10^{-2} mm) were glued with a spot of silver paste on the c faces, allowing both electrical contacts for dielectric measurements, and maintenance of the sample in a chosen position.

Figure 1 illustrates the DKDP sample in a vertical constant thermal gradient $\boldsymbol{G}_e$. The angle between the c axis and $\boldsymbol{G}_e$ is denoted α. The angle between the represented quasi-planar phase front and the (001) plane is denoted β. It is important to note that the sample's

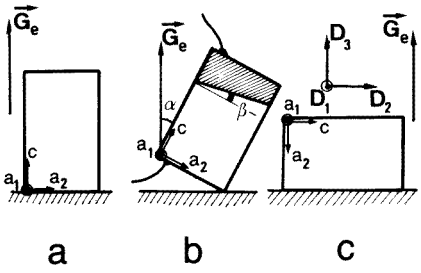

Figure 1. Schematic representation of the DKDP sample in a vertical thermal gradient $\boldsymbol{G}_e$. The lower face of the sample is in contact with a glass plate when (*a*) $\alpha = 0^\circ$ and (*c*) $\alpha = 90^\circ$ and (*b*) almost only with the helium exchange gas in the other cases.

boundaries are in contact with helium gas in all cases except for $\alpha = 0^\circ$ and $\alpha = 90^\circ$. In these cases the lower sample face is in contact with a glass plate which creates different thermal boundary conditions.

Different samples have been used in this study versus the angle α. When nothing is especially noted, the results presented correspond to a sample with dimensions $a_1 = 2.41$ mm, $a_2 = 4.71$ mm and $c = 9.02$ mm. The optical observations always performed along the directions D_1, D_2 (horizontal) and D_3 (vertical) show what happens in terms of domains and phase front. However, only the photographs along the a_1 direction (D_1) are of good quality and, for this reason, reported here.

3. Results

The phase coexistence looks very similar to those described previously with $\alpha = 0^\circ$ (Bornarel and Cach 1994) when α is less than 15°. The phase front appears in the lower face of the sample which is the cooler face, at a temperature of 211.9 K (all the temperatures given in this section result from measurement performed with a platinum resistor near the lower c face of the sample). Sometimes it crosses immediately the whole sample in the a_2 direction, but usually the first ferroelectric nucleus during a PF cycle is created in the lower corner of the sample. The nucleus phase front does not make an angle greater than 20° with the (001) plane. Then the dimension of the nucleus increases quickly in the a_2 direction until the ferroelectric region overruns all the lower part of the sample as illustrated by the schematic illustration with α equal to 15° in figure 2(*a*). The quasi-planar-shaped phase front moves along the c direction during the phase coexistence cycle. The angle β between the phase front and the (001) plane is greater when the front is nearer the corners of the sample than when it remains distant. In the case of figure 2(*a*), the β-value is constant (a few degrees) in the greater part of its motion except for 2 mm near the c faces.

When the angle α is greater than 15° and lower than 60°, the creation and the disappearance of the phase fronts in the sample's corners depend on the mechanical stresses and on the thermal distribution in these regions. Figure 2 gives some examples of different phase front shapes observed during PF (or FP) cycles for different α-values. In all the cases the phase front shape is simpler in the middle of the sample than in the corners. The angle β plotted versus the phase front position in the c direction in figure 2 corresponds to the part of the phase front in the median plane (010) of the sample. It can be observed that β is always a minimum in the middle of the sample. The curves showing the β variation demonstrate that, the greater the α-value, the greater is the corner memory on the phase front

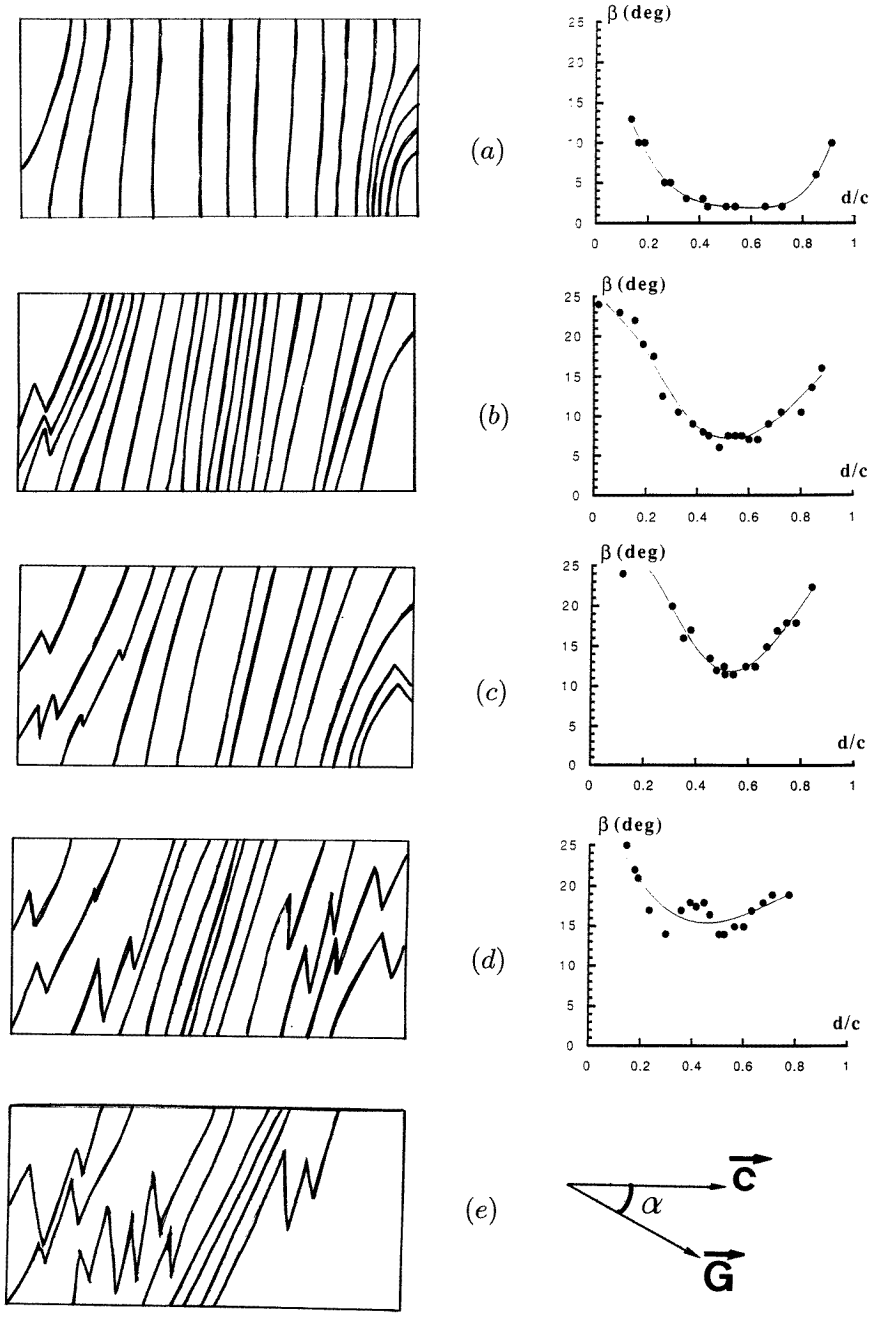

Figure 2. The photographs taken in an a_1 section have been exploited to summarize the phase front modification during a PF cycle with different α-values: (*a*) 15°; (*b*) 23°; (*c*) 47°; (*d*) 55°; (*e*) 61°. The left-hand representations show the phase front shape at different times during the PF cycle. The curves on the right give the angle β in the medium plane of the sample versus the position d in the c direction (c is the sample dimension in this direction).

shape; the sample's regions where a quasi-planar phase front can be observed decrease with increasing α. An α-value equal to 61° corresponds to a critical situation; the quasi-planar shape is only observable in the middle of the sample. For greater α, only zigzag phase front shapes are observed. Let us note also that β never exceeds 25°.

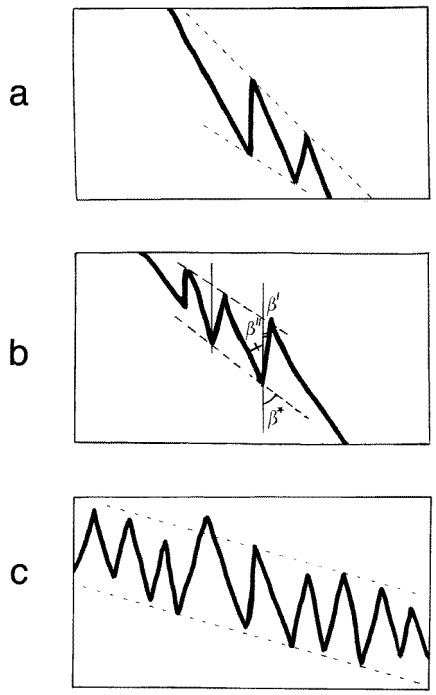

Figure 3. Schematic representation of the phase front shape in an a_1 section for different values of α: (*a*) 72°; (*b*) 74°; (*c*) 81°. The volume of the two phases (paraelectric and ferroelectric) is similar.

When the angle α is greater than 61° (in the given experimental case), the phase front trace in an a_1 section is always zigzag shaped. This phase front shape is shown in figure 3, for different α-values, in the case where the paraelectric and the ferroelectric regions exhibit the same volume in the sample. In a zigzag phase front, three angles can be defined: the angle between the (001) plane and the envelope of the zigzag denoted β^*, and the angles β' and β'' between the (001) plane and the quasi-planar parts of the phase front. Another parameter which characterizes the zigzag is the width of the coexistence region changing with the thermal gradient magnitude. It does not play a role in the present paper since the thermal gradient magnitude G_e is constant. As figures 2 and 3 have illustrated, the phase front shape changes very much with α and with β^*, β' and β'' too. These angle variations versus α are summarized in figure 4 with variation in $\beta(\alpha)$ previously defined. It is interesting to note that the graphs of $\beta(\alpha)$ (angle corresponding to quasi-planar phase fronts) and $\beta^*(\alpha)$ (angle corresponding to the envelope of the zigzag front) give a regular curve with a positive curvature between the origin (0, 0) and the point (90°, 90°). Moreover the values of β' and β'' are different for a given α because the edge of the zigzag is not symmetrical to the a_2 planes. In all cases, no quasi-planar part of the phase front ever makes an angle with the (001) plane exceeding 25°. This maximum value is observed in quasi-planar phase fronts as well as in zigzag phase fronts.

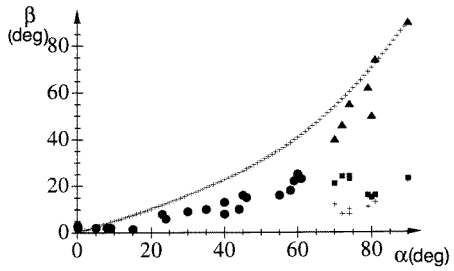

Figure 4. Variations in the different β with α: ● , angle between the quasiplanar phase front and (001) plane (defined in figure 1); ▲, β^* defined in figure 3(*c*); +, β' defined in figure 3(*c*); ■, β'' defined in figure 3(*c*). The continuous line of crosses illustrates the variation $\beta(\alpha)$ given by equation (3).

During a phase coexistence cycle, PF or FP, as illustrated in figure 2, the phase front shape remains unchanged during its translation in the medium region of the sample (except for the particular situation near α equal to 61°). It is observable with quasi-planar as well as with zigzag phase fronts. Then, the fact that the same phase front shape sometimes translates several millimetres with the temperature variation allows one to calculate the internal gradient G_i experimentally; the position d of a particular point of the phase front is drawn versus the temperature T measured near the lower face of the sample. The low cooling rate (less than 10^{-2} K min^{-1}) and the quasi-stability of the DKDP thermal conductivities during the transition lead one to suppose that the general shape of the temperature distribution remains unchanged in the middle of the sample for a given α situation. Only the positions of the isothermal surfaces are supposed to change. With these hypotheses, G_i can be obtained by calculating the $d(T)$ curve slope. The thermal external gradient G_e is directly measured by platinum resistors as previously described and then the ratio G_i/G_e is obtained. The fact that $\boldsymbol{G}_i$ is constant in the middle of the sample is best verified in the cases $\alpha = 0°$ and $\alpha = 90°$ and worst for α near to 60°. The role played by the sample corners and dimensions is evident and illustrated as follows. Different samples cut from the same crystal have been prepared with the same experimental procedure and are studied when α is equal to 90°. In one case, the same sample is set in two different positions related to $\boldsymbol{G}_e$. Figures 5 and 6 summarize the results obtained with four sample arrangements denoted s_1, s_2, s_3, s_4. The photographs in figure 5 performed along the a_1 axis show the zigzag trace in the middle of the sample and two photographs performed along the a_2 axis show straight lines which are a projection in the (010) plane of the zigzag. In figure 6, particular points of the phase front (an edge for example) are defined and their displacement d versus temperature is plotted. The linear dependences demonstrate that $\boldsymbol{G}_i$ is constant in the medium region of samples. Table 1 gives, for each case, the sample dimensions in the directions D_1, D_2 and D_3 defined in figure 1, and also the calculated values of the ration G_i/G_e ($\boldsymbol{G}_e$ is along D_3). These results will be discussed in the last section of the present paper. If the internal thermal gradient is constant in the middle of the samples, this is not the case near the sample boundaries, especially in the corners. A good illustration is given in figure 7. Figure 7(*a*) corresponds to the appearance of the phase front during a FP cycle on the upper face of the sample in contact with the helium exchange gas (with $G_e = 2.5$ K mm^{-1}). The photographs of the a_1 and a_2 sections show that the zigzags become straight lines in the sample at approximately 1 mm deep and curved lines nearer the sample's face defining the range of the corners on the thermal isotherms. Figure 7(*b*)

corresponds to the disappearance of the phase front on the lower face which is in contact with a glass window whose thermal conductivity is almost similar to that of the DKDP sample. Then the zigzags become straight lines at very small distances from the sample face. Furthermore the last ferroelectric regions are situated not only in the sample corners but also in other places of the sample face which proves that the isotherms inside the sample are almost planes perpendicular to $\boldsymbol{G}_e$ even near the sample boundary. The importance of the sample's thermal boundaries conditions is clearly illustrated by the previous results.

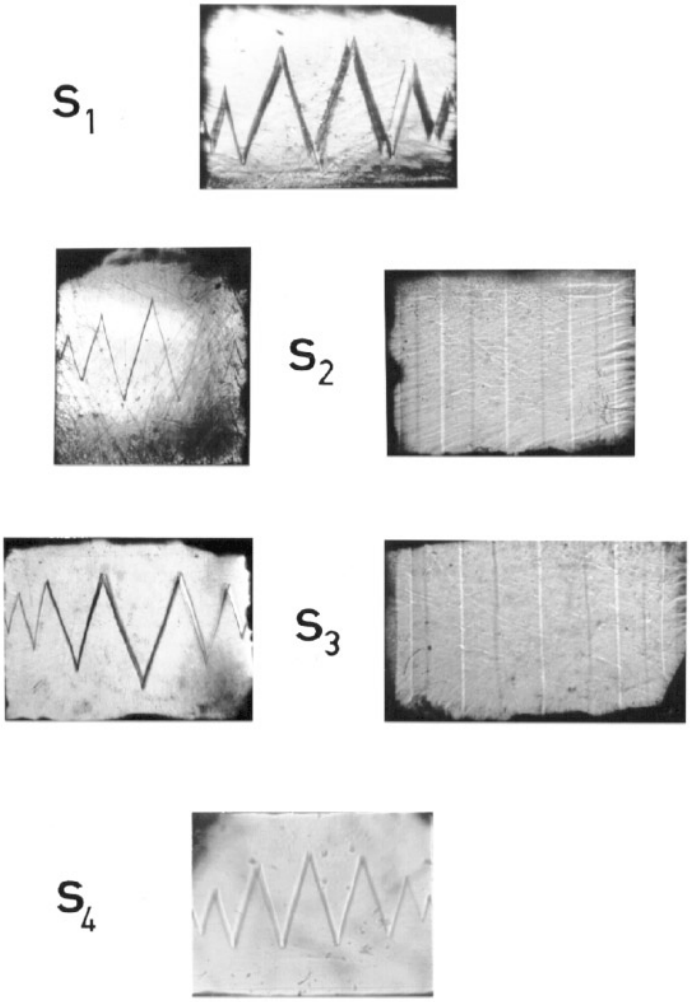

Figure 5. Photographs of the phase front traces in an a_1 section for samples s_1, s_2, s_3 and s_4 defined in the table 1. In cases s_2 and s_3, photographs along the a_2 direction are also given.

4. Discussion

The results presented in this paper confirm the existence of different shapes of the phase front during DKDP phase coexistences. Furthermore the existence of a critical angle between a planar region of the phase front and the (001) plane is also clearly proved. Very interesting

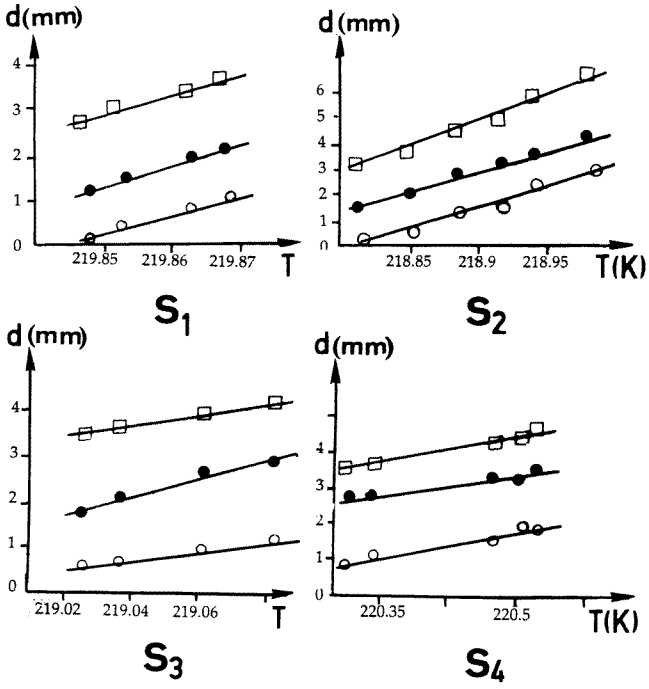

Figure 6. Using photographs such as those in figure 5, the position of a determined point of the zigzag phase front near the sample middle is plotted versus the temperature (measured near the lower sample's face): □, and ○ , the edge of the zigzag in the middle; ● , the upper edge nearest the sample boundary.

Table 1. The samples s_i as represented in figure 8(*b*) with G_e along the vertical direction. The experimental values of G_i/G_e are deduced from the $d(T)$ curves in figure 6 with $G_e = 0.2$ K mm^{-1}. The calculated values of G_i/G_e are obtained with the help of equation (4).

Sample	Dimensions (mm) $D_1 \times D_2 \times D_3$	G_i/G_e Experiment	G_i/G_e Calculation
s_1	$9.12 \times 6.32 \times 4.55$	0.125	0.16
s_2	$4.55 \times 6.32 \times 9.12$	0.35	0.36
s_3	$4.40 \times 7.39 \times 5.55$	0.30	0.23
s_4	$1.50 \times 7.39 \times 5.55$	1.25	0.4

models can be proposed to describe the phase front interface. This needs to minimize the electrostatic energy, the mechanical energy and the chemical energy, to take the sample boundaries into account as well as the energy of the interface itself. It is easy to demonstrate rapidly that the electrostatic energy is weaker than the other energies.

A first model was proposed by Kvitek (1996) who calculated the mechanical energy in the sample using Khatchaturyan's (1983) idea and Roitburd's (1993) work, the chemical energy, and the surface energy of the phase front. This first theoretical analysis of the zigzag-shaped interface allows us to explain the critical angles β^* in such a typical interface. Other improvements in the model are in progress: trying to dissociate the surface energy

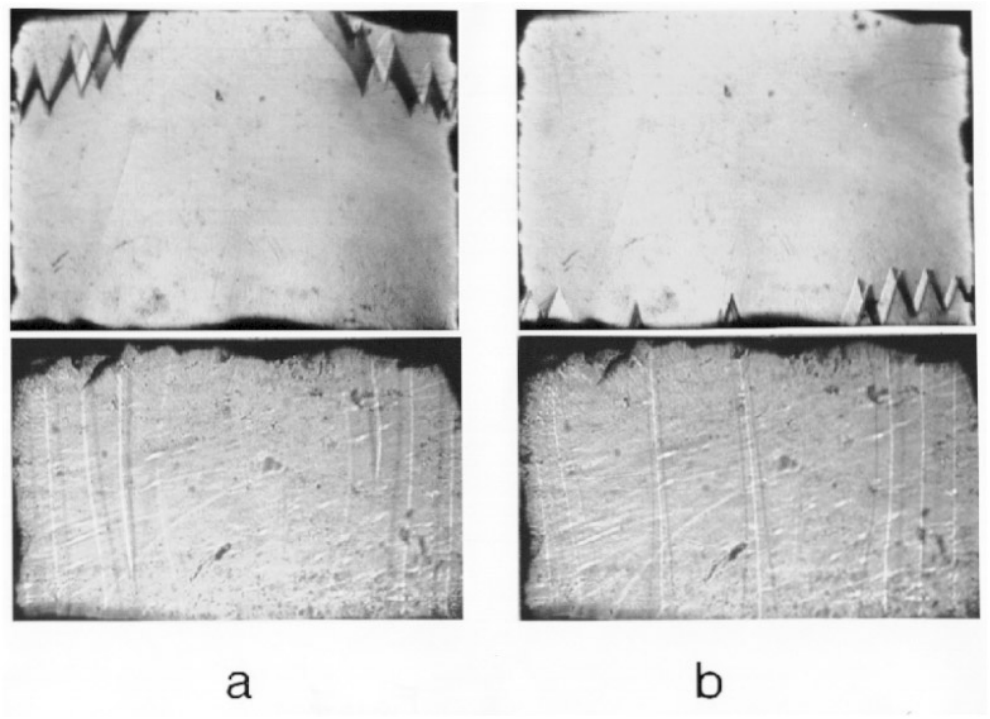

Figure 7. Photographs of the phase front during a FP cycle along a_1 (upper) and a_2 (lower) directions: (*a*) appearance of the phase front near the a_2 face on contact with helium gas; (*b*) disappearance of the phase front on the a_2 face on contact with a glass support.

of the planar regions from the energy of the zigzag edges, and testing the model versus the magnitude of the thermal gradient G_i. These will be published soon.

The aim of the following discussion is only to elucidate the role of the temperature distribution inside the sample because it is very useful to take it into account in all models near the transitions.

The parallelepipedic samples are set in an external thermal gradient $\boldsymbol{G}_e = \boldsymbol{\nabla} T_e$. The simplest model to describe the internal thermal distribution approximates the parallelepipedic sample to an ellipsoid. In this case the thermal distribution is a thermal gradient $\boldsymbol{G}_i = \boldsymbol{\nabla} T_i$ with a very simple relation between $\boldsymbol{G}_i$ and $\boldsymbol{G}_e$ (Landau and Lifchitz 1969):

$$\boldsymbol{\nabla} T_i = \boldsymbol{\kappa}\, \boldsymbol{\nabla} T_e \tag{1}$$

where $\boldsymbol{\kappa}$ is a second-order symmetric tensor which is a function of the ellipsoid shape and of the ratio p of the internal conductivity to the external conductivity: $p = \sigma_i/\sigma_e$. Taking into account the experimental measurements on the DKDP conductivity σ_i (Strukov and Belov 1992, Begunkova and Shubin 1983), it is possible to approximate σ_i by a scalar with the same value in the paraelectric and the ferroelectric phases at the phase transition. The normals of the sample faces define an orthogonal coordinate system corresponding to the principal axes A, B, C, of the ellipsoid as shown in figure 8. A, B and C are numbers without a dimension proportional to the ellipsoid parameters. Equation (1) gives by projection along each axis

$$(\boldsymbol{\nabla} T_i)_A = \kappa_A (\boldsymbol{\nabla} T_e)_A \tag{2}$$

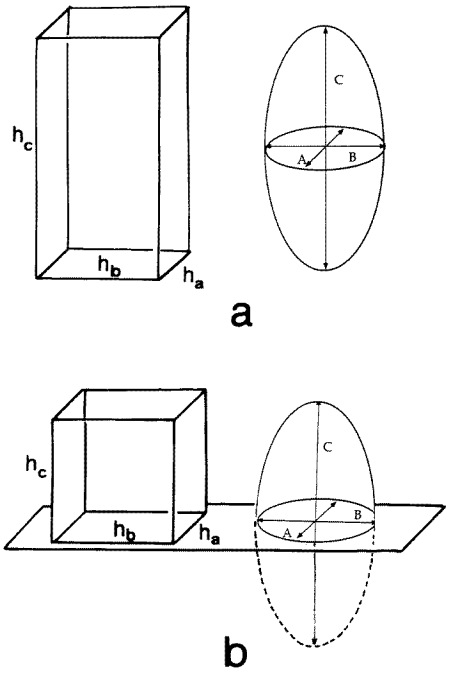

Figure 8. Representation of DKDP samples and the ellipsoids taken in the first-approximation model for thermal repartition: (*a*) sample surrounded by the helium exchange gas; (*b*) the lower face of the sample is in contact with a glass support. *A*, *B*, *C* are the outer dimensions and *h* has the dimension of a length.

with

$$\kappa_A = \frac{1}{1+(p-1)n_A}$$

$$n_A = \frac{ABC}{2}\int_0^\infty \frac{\mathrm{d}s}{(s+A^2)R}$$

$$R = [(s+A^2)(s+B^2)(s+C^2)]^{1/2}$$

and similar relations along *B* and *c* axes. It is possible to note that the ellipsoid volume does not play a role; only the relative ratio between *A*, *B* and *C* does. Because the values of κ_A, κ_B and κ_C are different, the internal thermal gradient $\boldsymbol{\nabla} T_i$ is not parallel to the external thermal gradient $\boldsymbol{\nabla} T_e$. To correlate this result with the experimental observations of the phase front versus α, the problem is approached as in figure 1 with two faces remaining in a vertical plane containing $\boldsymbol{G}_e$. Then *B* is the direction a_2 perpendicular to the figure, *A* and *C* corresponding to a_1 and *C* axes, respectively. With the relations

$$\boldsymbol{\nabla} T_i = \boldsymbol{G}_i = [(\boldsymbol{\nabla} T_i)_A, (\boldsymbol{\nabla} T_i)_C] = [G_i \sin\beta, G_i \cos\beta]$$

where β is the angle between $\boldsymbol{c}$ and $\boldsymbol{G}_i$, and

$$\boldsymbol{\nabla} T_e = \boldsymbol{G}_e = [(\boldsymbol{\nabla} T_e)_A, (\boldsymbol{\nabla} T_i)_C] = [G_e \sin\alpha, G_e \cos\alpha]$$

equation (2) allows us to obtain

$$\beta = \tan^{-1}\left[\frac{\kappa_A}{\kappa_C}\tan\alpha\right] \tag{3}$$

and

$$\frac{G_i}{G_e} = [(\kappa_C \cos\alpha)^2 + (\kappa_A \sin\alpha)^2]^{1/2}. \tag{4}$$

Using equation (3), classical values of σ_e for the helium gas giving $p = 20$, and the dimensions of the sample corresponding to figure 5 results giving $\kappa_A/\kappa_C = 0,5$, the theoretical dependence $\beta(\alpha)$ is drawn by a continuous line of crosses in figure 4. The outline is similar to that obtained with experimental points corresponding to quasi–planar phase fronts (α lower than 60°) and zigzag envelope (α greater than 60°) but the points do not fit in the curve, which can be explained as follows. The $\beta(\alpha)$ curve of the equation (3) shows that, in the model of an ellipsoid immersed in a constant thermal gradient $\boldsymbol{G}_e$, the internal gradient $\boldsymbol{G}_i$ is constant inside the sample but not parallel to $\boldsymbol{G}_e$ except for $\alpha = 0°$ and $\alpha = 90°$ as shown in figure 9. The angle $\alpha - \beta$ between $\boldsymbol{G}_i$ and $\boldsymbol{G}_e$ increases with increasing α until about 60° where $\alpha - \beta$ is equal to 20° and decreases for larger α-values, becoming zero at $\alpha = 90°$. Then the curve $\beta(\alpha)$ (continuous line of crosses) in figure 4 corresponds to the isotherm positions in the middle of the sample. The chemical energy is minimized when the quasi-planar front (for $\alpha < 60°$) is an isotherm, but the mechanical energy is minimized when the phase front is in the (001) plane. It can be seen that the result of minimization of the total energy leads to an intermediate position of the phase front. The fact that the zigzag shape begins at the maximum value of $\alpha - \beta$ is noted but not discussed in the present paper as previously explained.

Equation (4) allows one to draw the variation in the ratio G_i/G_e versus α as shown in figure 10 (for $p = 10$ and $p = 20$). The experimental results and the theoretical curves both decrease with increasing α without being quantitatively in agreement. The important effect of the p-values is noticeable and a careful study will need accurate knowledge of the conductivities and also the existence of the same thermal boundary conditions for all α-values. Equation (4) has also been used to calculate G_i/G_e with figure 8(b) conditions in figure 5 sample configurations ($\alpha = 90°$). The results are given in table 1. The discrepancies between the experimental and calculated results are not very large for samples s_1, s_2 and s_3 owing to the uncertainties in the conductivities. On the contrary the case of sample s_4 demonstrates that the ellipsoid model does not work for plate-shaped samples.

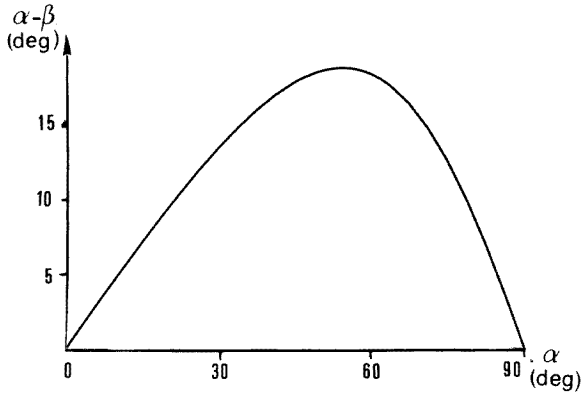

Figure 9. Variation in the angle $\alpha - \beta$ between the gradients $\boldsymbol{G}_e$ and $\boldsymbol{G}_i$ with α (ellipsoid model).

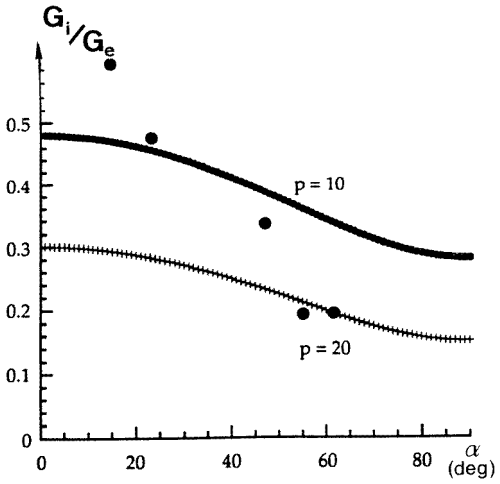

Figure 10. Variation in the ratio G_i/G_e with α in two cases of thermal conductivities: ■, $p = 10$; ++, $p = 20$. The experimental results are also given (●).

In our opinion, two reasons can explain this discrepancy in the plate-shaped case; the sample boundaries and especially the corners (for the G_e magnitude used) disturb the temperature distribution at distances similar to the sample thickness. Furthermore the results in table 1 are obtained with $\alpha = 90^\circ$, i.e. with very different thermal conditions for the two faces of the sample plate. It would be interesting to perform experiments, e.g. with plates between two glass windows, or on the contrary without any contact with a solid, suspended in helium gas with wires. This problem is important because, in many papers relating physical results near the transition, the thermal distribution inside the sample, and even the thermal boundary conditions are not described, whilst their role seems to be evident.

In conclusion the phase coexistence of DKDP samples has been studied in function of the orientation of the external thermal gradient $\boldsymbol{G}_e$ related to the sample. It has been clearly demonstrated that the phase front shape depends on this orientation and can be quasi-planar or with parallel bones (zigzag trace in a section). This phenomenon is explained by mechanical energy minimization and other papers will be published on this subject. However, if the phase front is not in the isothermal surfaces inside the sample, its shape is in strong interaction with the temperature repartition. Then it has been demonstrated above that, if the sample is in an external thermal gradient G_e, the temperature distribution in the middle of the sample is correctly described by a gradient G_i estimated by a simple ellipsoid model, excepted for a plate-shaped sample. On the contrary, the temperature distribution in the sample corners is more complex. It is an interesting problem and careful experiments are necessary to reach a better understanding of the nucleation which usually appears in these regions. Its influence on front shape, and on the thermal distribution has been illustrated. Other experiments on this point are in progress in our laboratory with the purpose of obtaining experimental results as significant as possible at the phase transition.

References

Aleshko-Ozhevskii O P 1982 *JETP Lett.* **35** 144
——1983 *Ferroelectrics* **48** 157
——1992 *Sov. Phys.–Solid State* **34** 499

Andrews S R and Cowley R A 1986 *J. Phys. C: Solid State Phys.* **19** 615
Bachheimer J P, Bastie P, Bornarel J, Dolino G and Vallade M 1981 *Proc. Int. Conf. on Solid–Solid Transformations* (Wairendale, PA: Metallurgical Society of AIME) p 1533
Bastie P, Bornarel J, Dolino G and Vallade M 1980 *Ferroelectrics* **26** 789
Begunkova A F and Shubin I F 1983 *Sov. J. Opt. Technol.* **50** 219
Bornarel J 1972 *J. Appl. Phys.* **43** 3845
——1987 *Ferroelectrics* **54** 585
Bornarel J and Cach R 1991 *Ferroelectrics* **124** 345
——1993 *J. Phys.: Condens. Matter* **5** 2977
——1994 *J. Phys.: Condens. Matter* **6** 1663
Bornarel J and Lajzerowicz J 1968 *J. Appl. Phys.* **39** 4339
Fousek J and Janovec V 1969 *J. Appl. Phys.* **40** 135
Khatchaturyan A G 1967 *Sov. Phys.–Solid State* **8** 2163
——1983 *Theory of Structural Transformations in Solids* (New York: Wiley)
Kvitek Z 1996 *J. Phys.: Condens. Matter* at press
Landau L and Lifchitz E 1969 *Fluids Mechanics* (Moscow: Mir)
Nelmes R J, Kuhs W F, Howard C J, Tibballs J E and Ryan T W 1985 *J. Phys. C: Solid State Phys.* **18** L1023
Reese W 1969 *Phys. Rev.* B **181** 2905
Roitburd A L 1993 *Phase Transitions* **45** 1
Sidnenko E C and Gladkii V V 1973 *Sov. Phys.–Solid State* **13** 2592
Strukov B A, Amin M and Kopchik V A 1968 *Phys. Status Solidi* **27** 741
Strukov B A, Amin A and Velichko I A 1972 *Sov. Phys.–Solid State* **13** 2085
Strukov B A and Belov A A 1992 *Ferroelectrics* **126** 299
Zeyen C, Meister H and Kley W 1976 *Solid State Commun.* **18** 621